

# Rotation mechanism of *Enterococcus hirae* V<sub>1</sub>-ATPase based on asymmetric crystal structures

Satoshi Arai<sup>1,2\*</sup>, Shinya Saijo<sup>2,3\*</sup>, Kano Suzuki<sup>1\*</sup>, Kenji Mizutani<sup>1,2,4</sup>, Yoshimi Kakinuma<sup>5</sup>, Yoshiko Ishizuka-Katsura<sup>6</sup>, Noboru Ohsawa<sup>6</sup>, Takaho Terada<sup>6</sup>, Mikako Shirouzu<sup>6</sup>, Shigeyuki Yokoyama<sup>6,7,8</sup>, So Iwata<sup>4,6</sup>, Ichiro Yamato<sup>2</sup> & Takeshi Murata<sup>1,6,9</sup>

**In various cellular membrane systems, vacuolar ATPases (V-ATPases) function as proton pumps, which are involved in many processes such as bone resorption and cancer metastasis, and these membrane proteins represent attractive drug targets for osteoporosis and cancer<sup>1</sup>. The hydrophilic V<sub>1</sub> portion is known as a rotary motor, in which a central axis DF complex rotates inside a hexagonally arranged catalytic A<sub>3</sub>B<sub>3</sub> complex using ATP hydrolysis energy, but the molecular mechanism is not well defined owing to a lack of high-resolution structural information. We previously reported on the *in vitro* expression, purification and reconstitution of *Enterococcus hirae* V<sub>1</sub>-ATPase from the A<sub>3</sub>B<sub>3</sub> and DF complexes<sup>2,3</sup>. Here we report the asymmetric structures of the nucleotide-free (2.8 Å) and nucleotide-bound (3.4 Å) A<sub>3</sub>B<sub>3</sub> complex that demonstrate conformational changes induced by nucleotide binding, suggesting a binding order in the right-handed rotational orientation in a cooperative manner. The crystal structures of the nucleotide-free (2.2 Å) and nucleotide-bound (2.7 Å) V<sub>1</sub>-ATPase are also reported. The more tightly packed nucleotide-binding site seems to be induced by DF binding, and ATP hydrolysis seems to be stimulated by the approach of a conserved arginine residue. To our knowledge, these asymmetric structures represent the first high-resolution view of the rotational mechanism of V<sub>1</sub>-ATPase.**

V-ATPases are thought to have originated from an ancestral enzyme in common with F-ATPases, which function as ATP synthases in mitochondria, chloroplasts and oxidative bacteria<sup>4,5</sup>. These ATPases possess an overall similar structure that is composed of a hydrophilic domain (V<sub>1</sub> and F<sub>1</sub>) and a membrane-embedded ion-transporting domain (V<sub>o</sub> and F<sub>o</sub>), and they have a similar reaction mechanism that occurs through rotation<sup>1</sup>. The rotational catalysis of F<sub>1</sub>-ATPase has been investigated in detail, and the molecular mechanism has been proposed on the basis of crystal structures of the complex from bovine<sup>6–9</sup>, yeast<sup>10–12</sup> and bacteria<sup>13,14</sup>, and extensive single-molecule observation of the rotation<sup>15–17</sup>. Similar V<sub>1</sub>-ATPase experiments have been conducted using the *Thermus thermophilus* enzyme, which functions physiologically as an ATP synthase<sup>18</sup>. The crystal structures of the A<sub>3</sub>B<sub>3</sub> complex at 2.8 Å resolution<sup>19</sup> and the A<sub>3</sub>B<sub>3</sub>DF (V<sub>1</sub>) complex at low resolution (4.5–4.8 Å)<sup>20</sup> suggest differences in its structure and interactions compared to F<sub>1</sub>-ATPases. Single-molecule analyses of V<sub>1</sub>-ATPase also suggest differences in torque generation and the coupling scheme of the rotation mechanism as compared to F<sub>1</sub> (ref. 21).

*Enterococcus hirae* V-ATPase, which acts as a primary ion pump similar to eukaryotic V-ATPases, uniquely transports Na<sup>+</sup> or Li<sup>+</sup> instead of H<sup>+</sup> ions<sup>22–25</sup>. The enzyme is composed of nine subunits with amino acid sequences that are homologous to those of the corresponding subunits of eukaryotic V-ATPases<sup>26–28</sup> (Supplementary Fig. 1). In this study, we solved the first asymmetric structures of

A<sub>3</sub>B<sub>3</sub> and A<sub>3</sub>B<sub>3</sub>DF (V<sub>1</sub>) complexes at high resolution, which enabled the generation of a new model of the rotational mechanism.

The *E. hirae* A<sub>3</sub>B<sub>3</sub> complex was purified and crystallized in the absence of nucleotide. The crystal structure was solved at a resolution of 2.8 Å (Supplementary Table 1). The three catalytic A subunits (Eh-A) and the three non-catalytic B subunits (Eh-B) are alternatively arranged and form a hexagonal ring (Fig. 1a). The structures of these subunits comprise the amino-terminal β-barrel domain, the central α/β domain and the carboxy-terminal helical domain (Supplementary Figs 2 and 3). The three Eh-A or Eh-B subunits in the A<sub>3</sub>B<sub>3</sub> complex were shown to have similar secondary structures, but their three-dimensional conformations slightly differed (see Supplementary Fig. 4). We superimposed the N-terminal β-barrel region of the three Eh-A or Eh-B subunits to examine the conformational differences in the A<sub>3</sub>B<sub>3</sub> complex, because this β-barrel domain should be fixed to form an alternatively arranged ring. One of the three Eh-A subunits adopts a closed conformation (denoted as A<sub>C</sub>), which shifts the structure into the centre of the A<sub>3</sub>B<sub>3</sub> ring, whereas the other two Eh-A subunits adopt similar open conformations (denoted as A<sub>O</sub> and A<sub>O</sub>'), even though an α-helix (residues 261–275; designated as the 'arm') of the three Eh-A conformations was almost fixed (Fig. 1b and Supplementary Fig. 4). Similarly, one of the three Eh-B subunits shows a closed conformation (denoted as B<sub>C</sub>) compared to the others (denoted as B<sub>O</sub> and B<sub>O</sub>') (Fig. 1c). Thus, the A<sub>3</sub>B<sub>3</sub> hexamer assembled asymmetrically by adjacent A<sub>O</sub> and B<sub>O</sub>, A<sub>O</sub>' and B<sub>O</sub>' and A<sub>C</sub> and B<sub>C</sub> subunits, whereas the conserved nucleotide-binding sites were located between the three different combinations: A<sub>O</sub>B<sub>C</sub>, A<sub>O</sub>'B<sub>O</sub> and A<sub>C</sub>B<sub>O</sub>' pairs (Fig. 1d).

The nucleotide-binding sites, which are comprised of the phosphate-binding loop (P-loop: GXXXXGKT(S)), the N-terminal portion of the arm (Glu 261 and Arg 262) in Eh-A, and Arg 350 (the 'Arg-finger' in ATPases) in Eh-B, had three different conformations (Fig. 1i–k). Electron density for nucleotides in the three binding sites was not observed (Supplementary Fig. 5), consistent with the absence of nucleotide contamination (ADP and ATP) detected in our sample and nucleotide-free crystallization conditions. Thus, surprisingly, the A<sub>3</sub>B<sub>3</sub> complex, which is formed by three identical Eh-A and Eh-B subunits, demonstrated complete asymmetry without nucleotide binding (see Supplementary Fig. 6 for comparison with the symmetric structures of corresponding previously reported complexes of V- and F-ATPases). The observed asymmetric structure of nucleotide-free A<sub>3</sub>B<sub>3</sub> (designated as eA<sub>3</sub>B<sub>3</sub>) may provide new insights for understanding the cooperative nature of the rotary motor as described below.

Next, we crystallized the A<sub>3</sub>B<sub>3</sub> complex in the presence of a high concentration (5 mM) of the non-hydrolysable ATP analogue adenosine 5'-(β,γ-imino)triphosphate (AMP-PNP) with MgSO<sub>4</sub>, and solved the structure of nucleotide-bound A<sub>3</sub>B<sub>3</sub> (denoted as bA<sub>3</sub>B<sub>3</sub>) at

<sup>1</sup>Department of Chemistry, Graduate School of Science, Chiba University, 1-33 Yayoi-cho, Inage, Chiba 263-8522, Japan. <sup>2</sup>Department of Biological Science and Technology, Tokyo University of Science, 2641 Yamazaki, Noda-shi, Chiba 278-8510, Japan. <sup>3</sup>RIKEN Spring-8 Center, 1-1-1 Kouto, Sayo, Hyogo 679-5148, Japan. <sup>4</sup>Department of Cell Biology, Faculty of Medicine, Kyoto University, Yoshidakonoe-cho, Sakyo-ku, Kyoto 606-8501, Japan. <sup>5</sup>Laboratory of Molecular Physiology and Genetics, Faculty of Agriculture, Ehime University, 3-5-7 Tarumi, Matsuyama, Ehime 790-8566, Japan. <sup>6</sup>RIKEN Systems and Structural Biology Center, 1-7-22 Suehiro-cho, Tsurumi, Yokohama 230-0045, Japan. <sup>7</sup>Department of Biophysics and Biochemistry, Graduate School of Science, The University of Tokyo, 7-3-1 Hongo, Bunkyo-ku, Tokyo 113-0033, Japan. <sup>8</sup>Laboratory of Structural Biology, Graduate School of Science, The University of Tokyo, 7-3-1 Hongo, Bunkyo-ku, Tokyo 113-0033, Japan. <sup>9</sup>JST, PRESTO, 1-33 Yayoi-cho, Inage, Chiba 263-8522, Japan.

\*These authors contributed equally to this work.

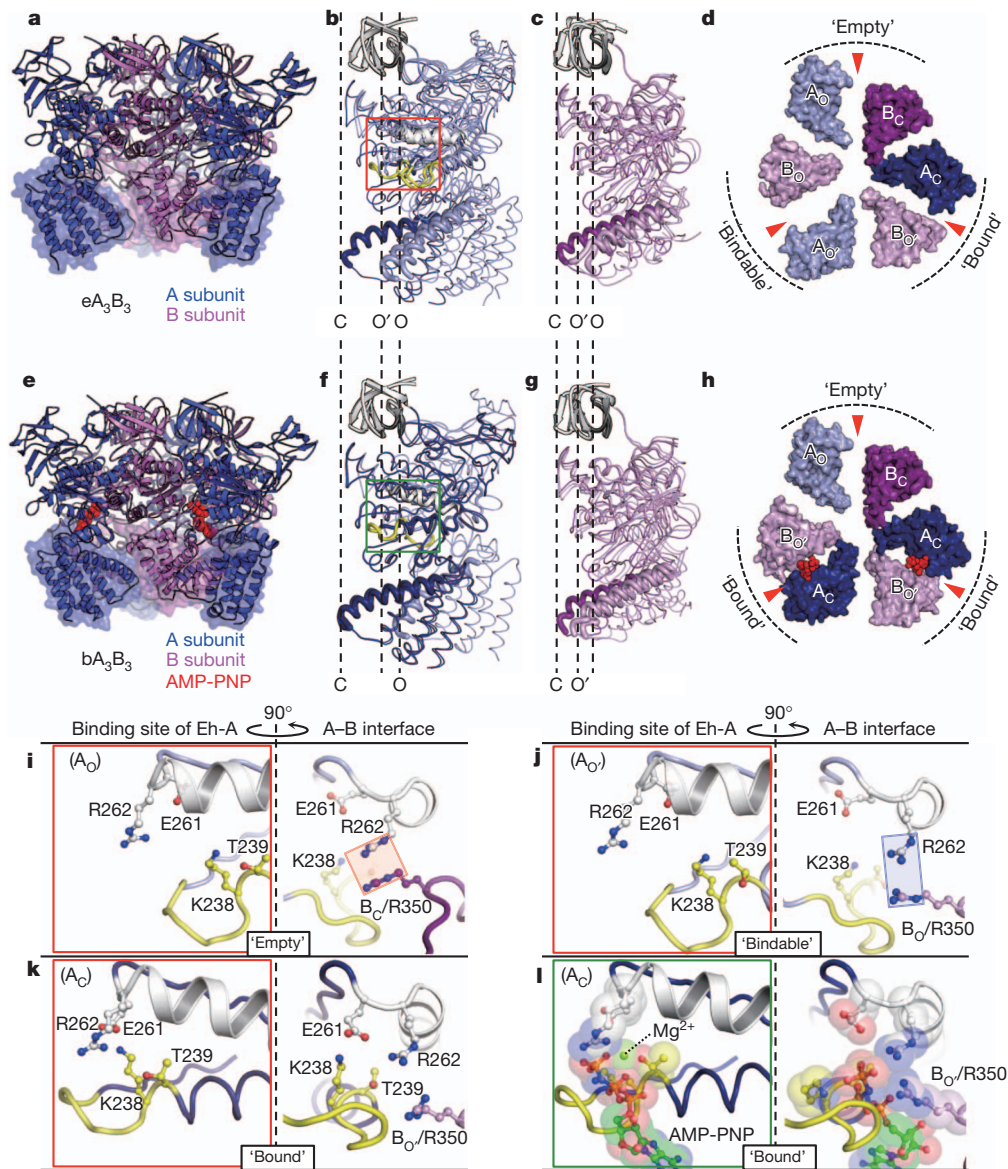


**Figure 1 | Structure of the  $A_3B_3$  complex.** **a**, Side view of the nucleotide-free  $A_3B_3$  structure ( $eA_3B_3$ ). **b**, **c**, Superimposed structures at the N-terminal  $\beta$ -barrel (white) of three structures of Eh-A (**b**) and Eh-B (**c**) in  $eA_3B_3$ . Open (O and O') and closed (C) conformations of Eh-A and Eh-B are shown in light and dark colours, respectively. The P-loop and arm are shown in yellow and white, respectively. **d**, Top view of the C-terminal domain (shown in **a** as transparent

surface) of  $eA_3B_3$  from the N-terminal  $\beta$ -barrel side. Red arrows indicate the nucleotide-binding sites. **e**–**h**, Structures of the AMP-PNP-bound  $A_3B_3$  complex ( $bA_3B_3$ ) viewed and coloured as in **a**–**d**. **i**–**l**, Magnified nucleotide-binding sites with conserved residues, corresponding to red (**b**) and green (**f**) boxes. Right panels show the A–B interfaces rotated  $90^\circ$  around a vertical axis from the left panels.

a resolution of  $3.4 \text{ \AA}$  (Supplementary Table 1). Two strong electron density peaks for AMP-PNP:Mg were found at the nucleotide-binding pockets in two Eh-AB pairs (Supplementary Fig. 7). The other AB pair, in which no density for nucleotide was found, was very similar to the  $A_OB_C$  pair in  $eA_3B_3$  (root mean squared deviation (r.m.s.d.) =  $0.477 \text{ \AA}$ ). We designated these  $A_OB_C$  pairs as the 'empty' form on the basis of their apparent very low affinity for AMP-PNP:Mg. The two AMP-PNP:Mg-bound AB pairs were very similar to each other (r.m.s.d. =  $0.511 \text{ \AA}$ ), and were also similar to the  $A_CB_O$  pair in  $eA_3B_3$  (r.m.s.d. =  $0.683 \text{ \AA}$  and  $0.719 \text{ \AA}$ ) except for the side-chain conformations that directly interacted with AMP-PNP:Mg (Fig. 1k, l and Supplementary Fig. 8). This finding suggests that the  $A_CB_O$  pair of  $eA_3B_3$  takes the ATP-bound form even in the absence of nucleotide; we designated these  $A_CB_O$  pairs as the 'bound' form. Furthermore, the more open  $A_OB_O$  pair of  $eA_3B_3$  seemed to bind AMP-PNP:Mg and to change to the bound form of  $bA_3B_3$ ; that is, binding of AMP-PNP:Mg induced the conformational change of  $A_3B_3$  from the  $A_OB_O$  pair to

the  $A_CB_O$  pair (see Supplementary Video 1). We designated this unique  $A_OB_O$  pair of  $eA_3B_3$  as 'bindable' form.

The reason that the empty form cannot bind AMP-PNP:Mg whereas the bindable form can is discussed here. The binding sites of empty and bindable forms are very similar except for the topologies of the Arg-fingers (Arg 350): the Arg-finger of closed Eh-B ( $B_C$ ) in the empty conformation was closer to Arg 262 than that of open Eh-B ( $B_O$ ) in the bindable conformation (Fig. 1i, j, red and blue boxes), which may prevent AMP-PNP:Mg binding. The conformation of Eh-B may regulate ATP-binding affinity by the Arg-finger (Arg 350) at the binding sites. Thus, these asymmetric structures suggest that the formation of the  $A_3B_3$  hexamer ring imposes a restriction (stress) on the Eh-AB pair to induce conformational changes (strains) that cooperatively generate one empty (ATP-unbound form), one bindable (ATP-accessible form) and one bound (ATP-bound form) conformation, which in turn determines the order of nucleotide binding in the ring in the right-handed rotational orientation viewed from the top of the  $V_1$  complex.

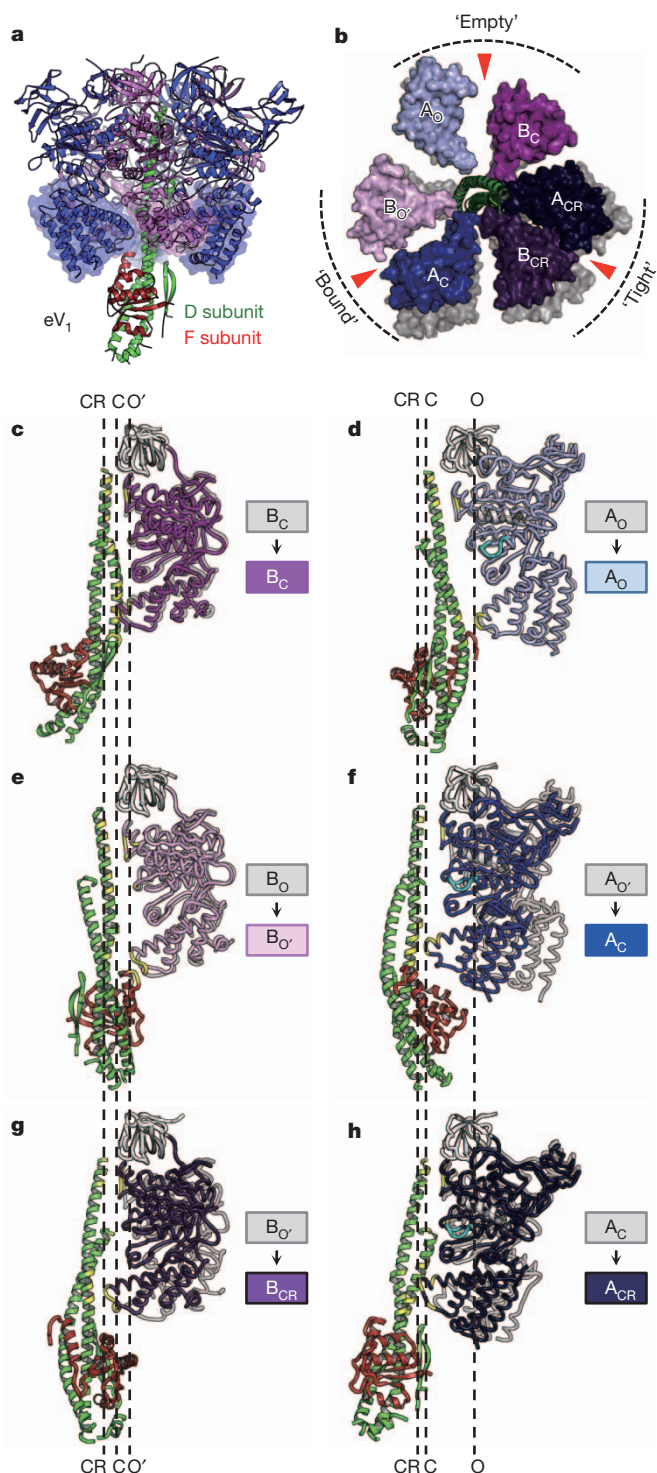


**Figure 2** | Comparison of the asymmetric structures of nucleotide-free  $A_3B_3DF$  and  $A_3B_3$  complexes. **a**, Side view of the nucleotide-free  $A_3B_3DF$  structure ( $eV_1$ ). **b**, Top views of the C-terminal domain of  $eV_1$  as in Fig. 1d, which is superimposed at the empty form onto that of transparent  $eA_3B_3$  (grey). Open (O and O'), closed (C) and closer (CR) conformations of Eh-A and -B are shown in light, dark and darker colours, respectively. **c–h**, Protein–protein interactions between  $A_3B_3$  and DF in  $eV_1$ . The  $B_C$  (**c**),  $A_O$  (**d**),  $B_{O'}$  (**e**),  $A_C$  (**f**),  $B_{CR}$  (**g**) and  $A_{CR}$  (**h**) with DF complex in  $eV_1$  are shown in side-viewed ribbon representation, which are compared with corresponding subunits (grey) of  $eA_3B_3$  superimposed as in **b**. The P-loop is shown in cyan. The residues with buried surface area  $>10 \text{ \AA}^2$ , as calculated by PDBEPIISA (<http://pdbe.org/pisa/>), are shown in yellow.

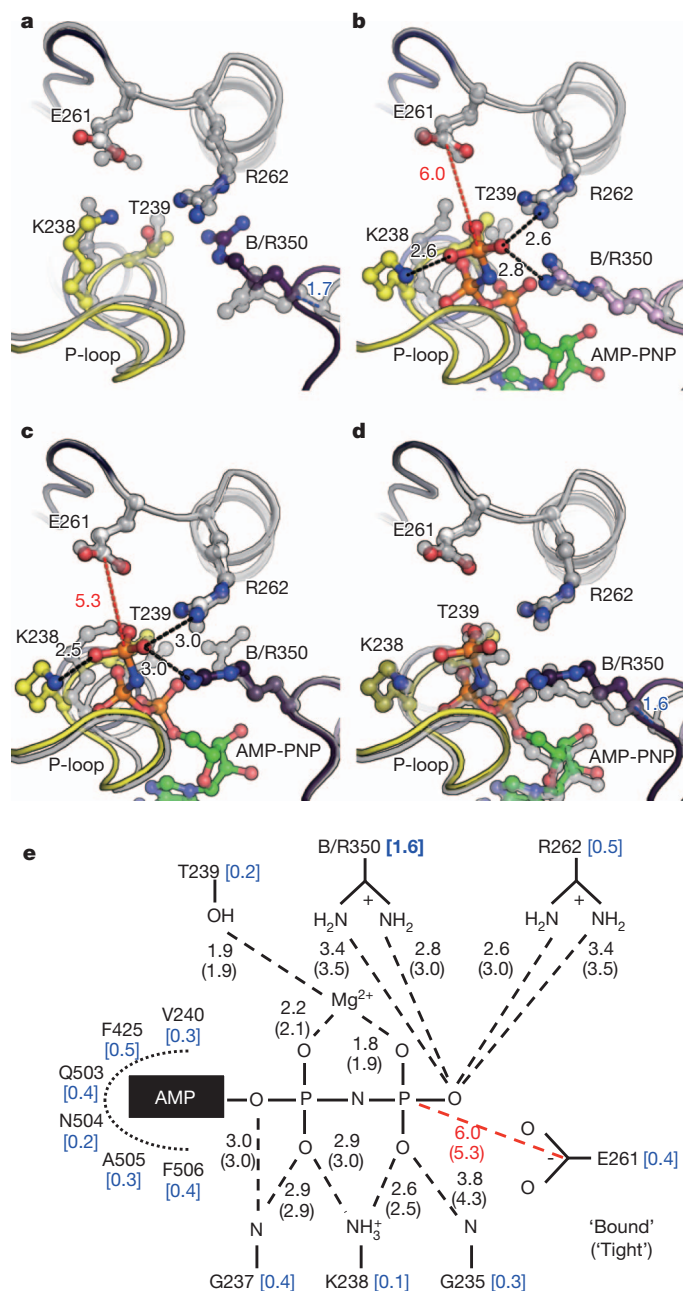


**Figure 3** | Comparison of the nucleotide-binding sites. **a–d**, The viewing position, colours and representations of the binding site correspond to those of the right columns in Fig. 1i–l. These structures were superimposed at Eh-A (residues 67–593) of the compared AB pairs. **a**, Tight form in  $eV_1$  (colour) compared with bound form in  $eA_3B_3$  (grey). **b**, Bound form in  $bV_1$  (colour) compared with bound form in  $eV_1$  (grey). **c**, Tight form in  $bV_1$  (colour) compared with tight form in  $eV_1$  (grey). **d**, Tight form in  $bV_1$  (colour) compared with bound form in  $bV_1$  (grey). The distances ( $\text{\AA}$ ) between atoms are shown with dotted lines. **e**, A schematic representation of the nucleotide-binding sites of  $bV_1$ . The distances ( $\text{\AA}$ ) between atoms in the bound form or tight form (shown in parentheses) are shown with dotted lines. The distances ( $\text{\AA}$ ) between  $C\alpha$ s in the superimposed structure (**d**) are shown in blue brackets.

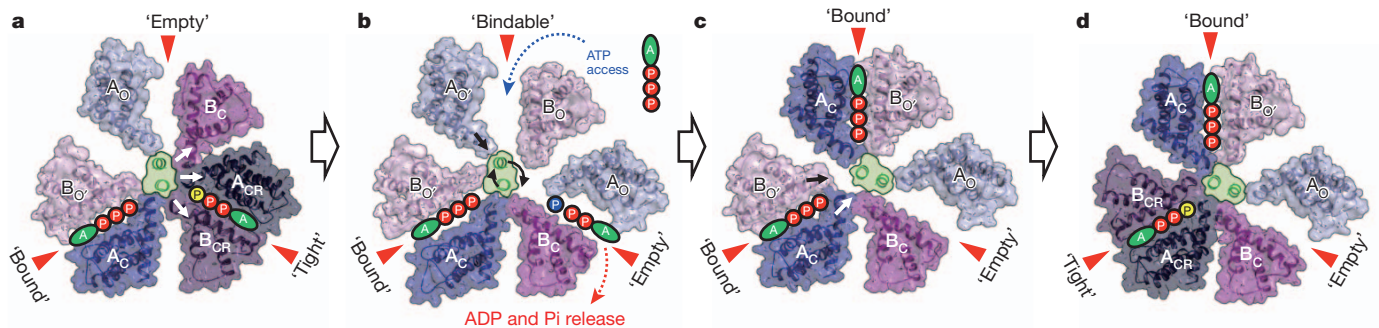


**Figure 4** | A model of the rotation mechanism of  $V_1$ -ATPase. **a–d**, The structure models are on the basis of the crystal structures of  $bV_1$  (**a** and **d**),  $eA_3B_3$  (**b**) and  $bA_3B_3$  (**c**) in this study. ATP with yellow 'P' in **a** and

**d** represents an ATP molecule that is committed to hydrolysis. The blue 'P' in **b** represents a Pi molecule after hydrolysis of ATP. See text for further details.

Next, we crystallized and solved the crystal structure of the nucleotide-free  $V_1$ -ATPase (denoted as  $eV_1$ ) at 2.2 Å resolution (see Supplementary Figs 9–11 and Supplementary Discussion for details). Eh-A and Eh-B assembled asymmetrically, similar to the  $A_3B_3$  complex, and a central axis composed of Eh-D and Eh-F penetrated into the cavity of the  $A_3B_3$  hexamer (Fig. 2a). Eh-D demonstrated a straighter conformation compared with that of the crystal structure of the DF complex<sup>3</sup>, but other features were very similar (Supplementary Fig. 12). The coiled-coil  $\alpha$ -helices of Eh-D interacted with several residues inside the  $A_3B_3$  complex by forming 19 polar interactions and 101 non-polar (van der Waals) interactions (Fig. 2c–h and Supplementary Fig. 13).

The structural differences between  $eA_3B_3$  and  $eV_1$  that should have been induced by interaction with the DF complex are compared in Fig. 2. The  $eV_1$  had an empty form ( $A_OB_O$ ) (r.m.s.d. = 0.544 Å) and a bound form ( $A_CB_O$ ) (r.m.s.d. = 0.699 Å), but the  $eV_1$ -bound form was positioned as the site of the  $eA_3B_3$ -bindable form when both empty forms were superimposed (Figs 1d and 2b and Supplementary Fig. 14). Therefore, the DF binding seemed to induce a change from the bindable form ( $A_OB_O$ ) of  $eA_3B_3$  to the bound form ( $A_CB_O$ ), similar to the conformational changes of the  $eA_3B_3$  induced by AMP-PNP binding (see Supplementary Videos 1 and 2). The remaining AB pair of  $eV_1$  represented a more tightly packed conformation composed of closer Eh-A and -B conformations approaching the centre of the  $A_3B_3$  ring, and this was not observed in the structure of the  $A_3B_3$  complex (Fig. 2g, h). We designated these new conformations of closer Eh-A and -B subunits and the tightly packed Eh-AB pair as the  $A_{CR}$  and  $B_{CR}$  subunits and 'tight' form, respectively. Therefore, DF complex binding seemed to change the bound form ( $A_CB_O$ ) of  $eA_3B_3$  to the tight form ( $A_{CR}B_{CR}$ ) by interacting with several Eh-A and -B residues (Fig. 2g, h and Supplementary Video 2).

These observations raise an intriguing question about the nature of the tight form, which occurs from the bound form by interaction with the DF complex. Figure 3a shows the nucleotide-binding site of the tight form ( $A_{CR}B_{CR}$ ) of  $eV_1$ , which was compared with that of the bound form ( $A_CB_O$ ) of  $eA_3B_3$ . In particular, the Arg-finger (Arg 350) of  $B_{CR}$  approached 1.7 Å closer to Arg 262 relative to that of  $B_O$  (Fig. 3a, blue dotted line). Thus, obtaining the structure of the nucleotide-bound  $V_1$ -ATPase is essential to understanding the effect of Arg-finger movement to the nucleotide. Crystals of  $eV_1$  were soaked in crystallization buffer with 200  $\mu$ M AMP-PNP:Mg (a concentration sufficient to inhibit activity), and the crystal structure of the nucleotide-bound  $V_1$ -ATPase (denoted as  $bV_1$ ) was solved to a resolution of 2.7 Å (Supplementary Table 2). The overall structure was very similar to that of  $eV_1$  (r.m.s.d. = 0.913 Å). A strong electron density peak for AMP-PNP:Mg was observed in the binding site of the bound and tight forms, but not in the empty form (Supplementary Fig. 15), indicating that the empty form has a low affinity for AMP-PNP:Mg, consistent with the observation of the empty form in  $bA_3B_3$ .

The  $\gamma$ -phosphate of AMP-PNP and  $Mg^{2+}$  were fixed by the Eh-A side chains of Lys 238, Thr 239 and Arg 262 and the Arg-finger (Arg 350) of Eh-B, similar to those of  $bA_3B_3$  (Fig. 3 and Supplementary Video 3). Superimposition of the binding site of the tight form onto that of the bound form in  $bV_1$  revealed small but significant differences between the two sites (Fig. 3b–e). In the tight form, movement of the Arg-finger (Arg 350) 1.6 Å closer to the  $\gamma$ -phosphate relative to the bound form (Fig. 3d, blue dotted line) caused the rotation of the AMP-PNP  $\gamma$ -phosphate. Subsequently, the  $\gamma$ -phosphate moved 0.7 Å closer to the conserved Glu 261 (see Supplementary Video 4), which is a crucial residue for hydrolysis of yeast  $V_1$ -ATPase<sup>29</sup>; the corresponding residue of  $F_1$ -ATPase interacts with the  $\gamma$ -phosphate oxygen of ATP via a water molecule and is assumed to cleave the  $\beta$ - $\gamma$  bond of ATP directly<sup>6,9,10,30</sup>. These findings suggest that hydrolysis of ATP is stimulated by this approach triggered by movement of the Arg-finger, which is induced by extensive protein–protein interactions between the DF complex and the C-terminal domains of Eh-A and Eh-B. To confirm the importance of the Arg-finger of Eh-B in ATP hydrolysis, we constructed three site-directed mutants of the Arg-finger and examined their biochemical properties (see Supplementary Table 3). The biochemical findings are consistent with the structural findings, in which hydrolysis of ATP is predicted to occur in the tight form induced by the Arg-finger approaching towards ATP. Therefore, we concluded that the obtained structure of  $bV_1$  represents an intermediate state of waiting for ATP hydrolysis in the catalytic cycle of  $V_1$ -ATPase.

The structures and conformational differences of the three Eh-A or B subunits are apparently different from those of the  $F_1$ -ATPases, although the nucleotide-binding-site structures of these ATPases are highly conserved (see Supplementary Figs 16, 17 and Supplementary Discussion). Here we summarize a possible model of the rotation mechanism of  $V_1$ -ATPase based on the asymmetric crystal structures in this study. Figure 4a shows the structure of the C-terminal domain surface of  $bV_1$  viewed from the top, in which two ATP:Mg molecules are bound in the bound and tight forms. Bound ATP in the tight form is awaiting ATP hydrolysis as described above. Hydrolysis of ATP seems to initiate the reaction as a trigger. New ATP molecules are unable to bind to the empty form because of its low affinity for ATP. Therefore, to continue the reaction, certain structural changes in the tight form should be induced by the conversion to ADP and Pi. If the effects of DF binding are ignored, the conformation of  $A_3B_3$  in  $V_1$ -ATPase may change (return) to  $eA_3B_3$  (ground structure of  $A_3B_3$  complex) in a cooperative manner, as shown in Fig. 4b: the bound form remains stabilized by the bound ATP:Mg, the empty and tight forms in  $V_1$  may change to the bindable form able to bind ATP and the empty form with low affinity for ATP, respectively. However, the extensive protein–protein interactions between the DF and  $A_{CR}B_{CR}$  pair (tight form) may prevent this conformational change within the  $A_3B_3$ , indicating that an intermediate state should exist in place of the state of Fig. 4b. In the next step, the rotation of the DF complex seems

to be induced by ATP binding to the bindable form, or to the corresponding conformation in the intermediate state in which Eh-B, with its Arg-finger, seems to adopt an open conformation similar to  $B_O$  to enable ATP binding. Subsequently, the conformation changes to  $bA_3B_3$ , which binds ATP:Mg molecules in two bound forms, and the DF complex rotates (Fig. 4c). Finally, the older bound form changes to the tight form, induced by DF binding (Fig. 4d and Supplementary Video 3). Simultaneously, hydrolysis of ATP is again enhanced by the approach of the Arg-finger caused by the conformational change, and the enzyme reverts to its initial state, as in Fig. 4a. To understand the rotational mechanism of  $V_1$ -ATPase more precisely, further investigations should be undertaken, such as additional structural studies, molecular simulations and single-molecule observation of the rotation.

## METHODS SUMMARY

**Sample preparation.** The  $A_3B_3$  and DF complexes of *E. hirae* were expressed using an *Escherichia coli* cell-free protein expression system and purified as previously described<sup>23</sup>. Eh- $V_1$  ( $A_3B_3$ DF) was purified by gel filtration after incubation of Eh- $A_3B_3$  with an excess concentration (fivefold) of Eh-DF.

**Crystallization, data collection and structure determination.** Crystals of nucleotide-free  $A_3B_3$  ( $eA_3B_3$ ), nucleotide-bound  $A_3B_3$  ( $bA_3B_3$ ), nucleotide-free  $V_1$  ( $eV_1$ ) and nucleotide-bound  $V_1$  ( $bV_1$ ) were grown by sitting drop vapour diffusion method under the conditions described in the Methods. Diffraction data were collected from a single cryo-cooled crystal on BL41XU at SPring-8 (Harima, Japan) and NW12A, NE3A and BL1A at Photon Factory (Tsukuba, Japan). The structures of  $eA_3B_3$ ,  $bA_3B_3$  and  $bV_1$  were solved by molecular replacement using the crystal structures of *T. thermophilus*  $A_3B_3$  complex (PDB accession 3GQB)<sup>19</sup>,  $A_3B_3$  part in  $eV_1$ , and whole  $eV_1$  as search models. The structure of  $eV_1$  was solved by molecular replacement with single-wavelength anomalous diffraction using the structures of  $eA_3B_3$  and Eh-DF (PDB accession 3AON), which were superimposed onto *T. thermophilus*  $V_1$ -ATPase (PDB accession 3A5C)<sup>20</sup>. Data collection and refinement statistics are summarized in Supplementary Tables 1 and 2.

**Full Methods** and any associated references are available in the online version of the paper.

Received 1 May; accepted 8 November 2012.

Published online 13 January 2013; corrected online 30 January 2013 (see full-text HTML version for details).

- Forgac, M. Vacuolar ATPases: rotary proton pumps in physiology and pathophysiology. *Nature Rev. Mol. Cell Biol.* **8**, 917–929 (2007).
- Arai, S. *et al.* Reconstitution *in vitro* of the catalytic portion (Ntp $A_3$ - $B_3$ -D-G complex) of *Enterococcus hirae* V-type  $Na^+$ -ATPase. *Biochem. Biophys. Res. Commun.* **390**, 698–702 (2009).
- Saijo, S. *et al.* Crystal structure of the central axis DF complex of the prokaryotic V-ATPase. *Proc. Natl Acad. Sci. USA* **108**, 19955–19960 (2011).
- Walker, J. E. ATP synthesis by rotary catalysis (Nobel Lecture). *Angew. Chem. Int. Edn Engl.* **37**, 2308–2319 (1998).
- Mulkidjanian, A. Y., Makarova, K. S., Galperin, M. Y. & Koonin, E. V. Inventing the dynamo machine: the evolution of the F-type and V-type ATPases. *Nature Rev. Microbiol.* **5**, 892–899 (2007).
- Abrahams, J. P., Leslie, A. G., Lutter, R. & Walker, J. E. Structure at 2.8 Å resolution of F<sub>1</sub>-ATPase from bovine heart mitochondria. *Nature* **370**, 621–628 (1994).
- Menz, R. I., Walker, J. E. & Leslie, A. G. Structure of bovine mitochondrial F<sub>1</sub>-ATPase with nucleotide bound to all three catalytic sites: implications for the mechanism of rotary catalysis. *Cell* **106**, 331–341 (2001).
- Kagawa, R., Montgomery, M. G., Braig, K., Leslie, A. G. W. & Walker, J. E. The structure of bovine F<sub>1</sub>-ATPase inhibited by ADP and beryllium fluoride. *EMBO J.* **23**, 2734–2744 (2004).
- Bowler, M. W., Montgomery, M. G., Leslie, A. G. W. & Walker, J. E. Ground state structure of F<sub>1</sub>-ATPase from bovine heart mitochondria at 1.9 Å resolution. *J. Biol. Chem.* **282**, 14238–14242 (2007).
- Kabaleeswaran, V., Puri, N., Walker, J. E., Leslie, A. G. W. & Mueller, D. M. Novel features of the rotary catalytic mechanism revealed in the structure of yeast F<sub>1</sub> ATPase. *EMBO J.* **25**, 5433–5442 (2006).
- Kabaleeswaran, V. *et al.* Asymmetric structure of the yeast F<sub>1</sub> ATPase in the absence of bound nucleotides. *J. Biol. Chem.* **284**, 10546–10551 (2009).
- Stock, D., Leslie, A. G. & Walker, J. E. Molecular architecture of the rotary motor in ATP synthase. *Science* **286**, 1700–1705 (1999).
- Shirakihara, Y. *et al.* The crystal structure of the nucleotide-free  $\alpha 3\beta 3$  subcomplex of F<sub>1</sub>-ATPase from the thermophilic *Bacillus* PS3 is a symmetric trimer. *Structure* **5**, 825–836 (1997).
- Cingolani, G. & Duncan, T. M. Structure of the ATP synthase catalytic complex (F<sub>1</sub>) from *Escherichia coli* in an autoinhibited conformation. *Nature Struct. Mol. Biol.* **18**, 701–707 (2011).
- Noji, H., Yasuda, R., Yoshida, M. & Kinosita, K. Direct observation of the rotation of F<sub>1</sub>-ATPase. *Nature* **386**, 299–302 (1997).
- Yasuda, R., Noji, H., Yoshida, M., Kinosita, K. & Itoh, H. Resolution of distinct rotational substeps by submillisecond kinetic analysis of F<sub>1</sub>-ATPase. *Nature* **410**, 898–904 (2001).
- Adachi, K. *et al.* Coupling of rotation and catalysis in F<sub>1</sub>-ATPase revealed by single-molecule imaging and manipulation. *Cell* **130**, 309–321 (2007).
- Toei, M. *et al.* Dodecamer rotor ring defines H<sup>+</sup>/ATP ratio for ATP synthesis of prokaryotic V-ATPase from *Thermus thermophilus*. *Proc. Natl Acad. Sci. USA* **104**, 20256–20261 (2007).
- Maher, M. J. *et al.* Crystal structure of  $A_3B_3$  complex of V-ATPase from *Thermus thermophilus*. *EMBO J.* **28**, 3771–3779 (2009).
- Numoto, N., Hasegawa, Y., Takeda, K. & Miki, K. Inter-subunit interaction and quaternary rearrangement defined by the central stalk of prokaryotic V<sub>1</sub>-ATPase. *EMBO Rep.* **10**, 1228–1234 (2009).
- Imamura, H. *et al.* Rotation scheme of V<sub>1</sub>-motor is different from that of F<sub>1</sub>-motor. *Proc. Natl Acad. Sci. USA* **102**, 17929–17933 (2005).
- Murata, T., Igarashi, K., Kakinuma, Y. & Yamato, I. Na<sup>+</sup> binding of V-type Na<sup>+</sup>-ATPase in *Enterococcus hirae*. *J. Biol. Chem.* **275**, 13415–13419 (2000).
- Murata, T., Yamato, I., Kakinuma, Y., Leslie, A. G. W. & Walker, J. E. Structure of the rotor of the V-Type Na<sup>+</sup>-ATPase from *Enterococcus hirae*. *Science* **308**, 654–659 (2005).
- Murata, T. *et al.* Ion binding and selectivity of the rotor ring of the Na<sup>+</sup>-transporting V-ATPase. *Proc. Natl Acad. Sci. USA* **105**, 8607–8612 (2008).
- Mizutani, K. *et al.* Structure of the rotor ring modified with N,N-dicyclohexylcarbodiimide of the Na<sup>+</sup>-transporting vacuolar ATPase. *Proc. Natl Acad. Sci. USA* **108**, 13474–13479 (2011).
- Murata, T., Yamato, I. & Kakinuma, Y. Structure and mechanism of vacuolar Na<sup>+</sup>-translocating ATPase from *Enterococcus hirae*. *J. Bioenerg. Biomembr.* **37**, 411–413 (2005).
- Yamamoto, M. *et al.* Interaction and stoichiometry of the peripheral stalk subunits NtpE and NtpF and the N-terminal hydrophilic domain of NtpI of *Enterococcus hirae* V-ATPase. *J. Biol. Chem.* **283**, 19422–19431 (2008).
- Zhou, M. *et al.* Mass spectrometry of intact V-type ATPases reveals bound lipids and the effects of nucleotide binding. *Science* **334**, 380–385 (2011).
- Liu, Q. *et al.* Site-directed mutagenesis of the yeast V-ATPase A subunit. *J. Biol. Chem.* **272**, 11750–11756 (1997).
- Dittrich, M., Hayashi, S. & Schulten, K. On the mechanism of ATP hydrolysis in F<sub>1</sub>-ATPase. *Biophys. J.* **85**, 2253–2266 (2003).

Supplementary Information is available in the online version of the paper.

**Acknowledgements** We thank J. E. Walker for his suggestions, especially through the structural studies of F<sub>1</sub>-ATPase. The synchrotron radiation experiments were performed at SPring-8 and Photon Factory (proposals 2008S2-001, 2011S2-005, 2009G660, 2009B1031 and 2012G132). We also thank the beamline staff at BL41XU of SPring-8 (Harima, Japan) and NE3A, NW12A and BL1A of Photon Factory (Tsukuba, Japan) for help during data collection. This work was supported by the Targeted Proteins Research Program, grants-in-aid (23370047, 23118705), Special Coordination Funds for Promoting Science and Technology from the Ministry of Education, Culture, Sports, Science and Technology of the Japanese government.

**Author Contributions** T.M. designed the study. S.A., Y.K. and N.O. constructed DNAs. Y.I.-K., T.T. and M.S. expressed and purified the proteins. K.S. and T.M. crystallized the proteins. S.A., S.S., K.S., K.M. and T.M. collected X-ray data. S.A., S.S. and K.M. processed and refined X-ray data. S.A. and K.S. performed functional analysis. S.A., S.S., I.Y. and T.M. analysed the results. S.A. and S.S. prepared figures and videos. T.M. wrote the paper. All authors discussed the results and commented on the manuscript. The study was managed by S.Y., S.I., I.Y. and T.M.

**Author Information** Atomic coordinates and structure factors for the  $A_3B_3$  and  $V_1$ -ATPase complexes have been deposited in the Protein Data Bank under the accession codes 3VR2 (nucleotide-free  $A_3B_3$  at 2.8 Å), 3VR3 (nucleotide-bound  $A_3B_3$  at 3.4 Å), 3VR4 (nucleotide-free  $V_1$ -ATPase at 2.2 Å), 3VR5 (nucleotide-free  $V_1$ -ATPase at 3.9 Å) and 3VR6 (nucleotide-bound  $V_1$ -ATPase at 2.7 Å). Reprints and permissions information is available at [www.nature.com/reprints](http://www.nature.com/reprints). The authors declare no competing financial interests. Readers are welcome to comment on the online version of the paper. Correspondence and requests for materials should be addressed to T.M. ([t.murata@faculty.chiba-u.jp](mailto:t.murata@faculty.chiba-u.jp)).

## METHODS

**Protein preparation.** An *Escherichia coli* cell-free protein expression system, as described elsewhere<sup>31</sup>, was used to synthesize the Eh-A<sub>3</sub>B<sub>3</sub> and DF complexes using a mixture of plasmids containing the corresponding genes. The expressed complexes were purified as previously described<sup>23</sup>. Selenomethionine-labelled Eh-A<sub>3</sub>B<sub>3</sub> and DF complexes were also prepared to facilitate X-ray structure determination. The sum of ATP and ADP contamination in 0.5 μM purified Eh-A<sub>3</sub>B<sub>3</sub> and DF complexes (denatured with 0.6 M perchloric acid) was estimated with a luciferin–luciferase assay<sup>32</sup>, after conversion of ADP to ATP using an ATP regeneration system<sup>3</sup> for 30 min at room temperature; ATP and ADP contamination was undetectable (less than 0.1 nM). The V<sub>1</sub>-ATPase (Eh-A<sub>3</sub>B<sub>3</sub>DF) was reconstituted and purified as follows: purified Eh-A<sub>3</sub>B<sub>3</sub> and Eh-DF in buffer A (20 mM Tris-HCl, pH 8.0, 150 mM NaCl and 2 mM dithiothreitol (DTT)) were mixed at a 1:5 molar ratio with the addition of MES (100 mM final concentration; pH 6.0), and were incubated with and without 0.2 mM AMP-PNP and 5 mM MgSO<sub>4</sub> for 1 h. Reconstituted V<sub>1</sub>-ATPase with and without AMP-PNP:Mg was purified using a HiLoad 16/60 Superdex 200 (GE Healthcare) column equilibrated with buffer B (20 mM MES, pH 6.5, 10% glycerol, 100 mM NaCl, 5 mM MgSO<sub>4</sub> and 2 mM DTT), respectively. Purified complexes were concentrated with an Amicon Ultra 30 K unit (Merck Millipore).

**Protein crystallization.** All crystallization trials were performed using the sitting-drop vapour diffusion method at 296 K. The crystals were soaked in cryoprotectant by incrementally increasing the glycerol concentration to 20%. The crystals were then mounted on cryo-loops (Hampton Research), flash-cooled and stored in liquid nitrogen.

(1) Eh-A<sub>3</sub>B<sub>3</sub> without nucleotide (eA<sub>3</sub>B<sub>3</sub>): Eh-A<sub>3</sub>B<sub>3</sub> crystals were obtained by mixing 0.5 μl protein solution (12 mg ml<sup>-1</sup> protein in buffer A) with 0.5 μl reservoir solution (0.1 M MES-Tris, pH 8.5, 24% PEG-3350 and 0.2 M ammonium acetate).

(2) Eh-A<sub>3</sub>B<sub>3</sub> with AMP-PNP:Mg (bA<sub>3</sub>B<sub>3</sub>): Eh-A<sub>3</sub>B<sub>3</sub> crystals were obtained by mixing 0.5 μl protein solution (11 mg ml<sup>-1</sup> protein in buffer A) supplemented with 5 mM AMP-PNP and 5 mM MgSO<sub>4</sub> with 0.5 μl reservoir solution (0.1 M HEPES, pH 7.5, 26% PEG-3350, and 0.2 M sodium chloride).

(3) V<sub>1</sub>-ATPase with AMP-PNP:Mg (eV<sub>1</sub>): V<sub>1</sub> crystals were obtained by mixing 0.5 μl protein solution (12 mg ml<sup>-1</sup> protein in the presence of 0.2 mM AMP-PNP in buffer B) with 0.5 μl reservoir solution (0.1 M Bis-Tris propane, pH 6.5, 19% PEG-3350 and 0.2 M sodium fluoride).

(4) V<sub>1</sub>-ATPase without nucleotide (eV<sub>1</sub>(L)): V<sub>1</sub> crystals were obtained by mixing 0.5 μl protein solution (10 mg ml<sup>-1</sup> protein in buffer B) with 0.5 μl reservoir solution (0.1 M Bis-Tris propane, pH 6.5, 20% PEG-3350 and 0.2 M sodium fluoride).

(5) V<sub>1</sub>-ATPase soaked with AMP-PNP:Mg (bV<sub>1</sub>): V<sub>1</sub> crystals that were obtained in (3) were soaked for 5 h in 0.1 M Bis-Tris propane, pH 6.5, 21% PEG-3350, 0.2 mM AMP-PNP (a concentration sufficient to inhibit the activity), 3 mM MgSO<sub>4</sub>, 0.2 M sodium chloride (replaced for sodium fluoride) and 20% glycerol.

**Structure determination.** All X-ray diffraction data were collected from a single crystal at a cryogenic temperature (100 K).

(1) Eh-A<sub>3</sub>B<sub>3</sub> without nucleotide (eA<sub>3</sub>B<sub>3</sub>): X-ray diffraction data were collected on beamline BL41XU (λ = 1.0000 Å) at SPring-8 (Harima, Japan). The collected data were processed to 2.8 Å using iMosflm<sup>33</sup> and then scaled by Scala from the CCP4 program suite<sup>34</sup>. The structure was solved by molecular replacement with MOLREP<sup>35</sup> using the poly-Ser model of A<sub>3</sub>B<sub>3</sub> complex from *T. thermophilus* (PDB accession 3GQB)<sup>19</sup> as a search model.

(2) Eh-A<sub>3</sub>B<sub>3</sub> with AMP-PNP:Mg (bA<sub>3</sub>B<sub>3</sub>): X-ray diffraction data were collected on beamline BL41XU (λ = 1.0000 Å) at SPring-8. The collected data were processed to 3.4 Å using iMosflm<sup>33</sup> and then scaled by Scala<sup>34</sup>. The structure was solved by molecular replacement with MOLREP<sup>35</sup> using the structure of Eh-A<sub>3</sub>B<sub>3</sub> in eV<sub>1</sub> as a search model.

(3) V<sub>1</sub>-ATPase with AMP-PNP:Mg (eV<sub>1</sub>): X-ray diffraction data were collected on beamline NW12A (λ = 0.97919 and 1.0000 Å) at Photon Factory (Tsukuba,

Japan). The collected data were processed and scaled to 2.6 and 2.2 Å using XDS<sup>36</sup>. The structure was solved by MR-SAD (molecular replacement with single-wavelength anomalous diffraction) using Phaser<sup>37</sup>. The partially refined A and B subunits from the structure of Eh-A<sub>3</sub>B<sub>3</sub> without nucleotide and the DF complex from *E. hirae* (PDB accession 3AON) were superimposed onto the V<sub>1</sub>-ATPase from *T. thermophilus* (PDB accession 3A5C)<sup>20</sup>. The superimposed model was used as an initial search model. The overall figure of merit (FOM =  $\sum P(x) \exp(ix) / \sum P(x)$ , in which  $P(x)$  is the probability distribution for the phase( $x$ )) was 0.45 using combined phases of SAD from selenium and molecular replacement at 3.0 Å.

(4) V<sub>1</sub>-ATPase without nucleotide (eV<sub>1</sub>(L)): X-ray diffraction data were collected on beamline NE3A (λ = 1.0000 Å) at Photon Factory. The collected data were processed to 3.9 Å using XDS. The structure was solved by molecular replacement with Phaser using the crystal structure of eV<sub>1</sub> as a search model.

(5) V<sub>1</sub>-ATPase soaked with AMP-PNP:Mg (bV<sub>1</sub>): X-ray diffraction data were collected on beamline BL1A (λ = 1.0000 Å) at Photon Factory. The collected data were processed to 2.7 Å using HKL2000 software (HKL Research). The structure was solved by molecular replacement with MOLREP using the crystal structure of eV<sub>1</sub> as a search model.

The atomic models were manually built using Coot<sup>38</sup> and iteratively refined using REFMAC5<sup>39</sup> (REFMAC5 and PHENIX<sup>40</sup> were used for refinement of eV<sub>1</sub>). The refined structures were validated with PROCHECK<sup>41</sup> and RAMPAGE<sup>42</sup>. The crystallographic and refinement statistics are summarized in Supplementary Tables 1 and 2. The r.m.s.d. values of superimpositions for each Eh-A, Eh-B or Eh-AB pair in the crystal structures of A<sub>3</sub>B<sub>3</sub> and V<sub>1</sub>-ATPase are listed in Supplementary Tables 4 and 5. Figures were prepared using PyMOL (The PyMOL Molecular Graphics System, Version 1.3, Schrodinger, LLC.)

**Characterization of the Arg-finger mutants.** Mutagenesis of the Arg-finger (Arg350Ala/Glu/Lys) of Eh-B was performed using the QuikChange site-directed mutagenesis kit (Agilent Technologies). The Arg350Ala Eh-B mutant could not be purified as a complex with Eh-A. The other mutants were purified as described above. Binding affinities between the Eh-A<sub>3</sub>B<sub>3</sub> mutants and the DF complex were measured using the Biacore T100 system (GE Healthcare) as described previously<sup>3</sup>. The dissociation constant ( $K_d$ ) was determined using BIAevaluation software (version 1.1), which uses the Langmuir isotherm model that assumes a 1:1 binding stoichiometry. ATPase activity was measured according to a previous report using the ATP-regeneration system<sup>3</sup>.

- Kigawa, T. *et al.* Preparation of *Escherichia coli* cell extract for highly productive cell-free protein expression. *J. Struct. Funct. Genomics* **5**, 63–68 (2004).
- Deluca, M. & McElroy, W. D. Purification and properties of firefly luciferase. *Methods Enzymol.* **57**, 3–15 (1978).
- Battye, T. G. G., Kontogiannis, L., Johnson, O., Powell, H. R. & Leslie, A. G. W. iMOSFLM: a new graphical interface for diffraction-image processing with MOSFLM. *Acta Crystallogr. D* **67**, 271–281 (2011).
- Collaborative Computational Project, Number 4. The CCP4 suite: programs for protein crystallography. *Acta Crystallogr. D* **50**, 760–763 (1994).
- Vagin, A. & Teplyakov, A. Molecular replacement with MOLREP. *Acta Crystallogr. D* **66**, 22–25 (2010).
- Kabsch, W. XDS. *Acta Crystallogr. D* **66**, 125–132 (2010).
- McCoy, A. J. *et al.* Phaser crystallographic software. *J. Appl. Crystallogr.* **40**, 658–674 (2007).
- Emsley, P. & Cowtan, K. Coot: model-building tools for molecular graphics. *Acta Crystallogr. D* **60**, 2126–2132 (2004).
- Murshudov, G. N., Vagin, A. A. & Dodson, E. J. Refinement of macromolecular structures by the maximum-likelihood method. *Acta Crystallogr. D* **53**, 240–255 (1997).
- Adams, P. D. *et al.* PHENIX: a comprehensive Python-based system for macromolecular structure solution. *Acta Crystallogr. D* **66**, 213–221 (2010).
- Laskowski, R. A., MacArthur, M. W. & Thornton, J. M. Validation of protein models derived from experiment. *Curr. Opin. Struct. Biol.* **8**, 631–639 (1998).
- Lovell, S. C. *et al.* Structure validation by C $\alpha$  geometry:  $\phi$ ,  $\psi$  and C $\beta$  deviation. *Proteins* **50**, 437–450 (2003).